



OPEN

## Histone modifications form a cell-type-specific chromosomal bar code that persists through the cell cycle

John A. Halsall<sup>1</sup>✉, Simon Andrews<sup>2</sup>, Felix Krueger<sup>2</sup>, Charlotte E. Rutledge<sup>1</sup>, Gabriella Ficiz<sup>3</sup>, Wolf Reik<sup>4</sup> & Bryan M. Turner<sup>1</sup>✉

Chromatin configuration influences gene expression in eukaryotes at multiple levels, from individual nucleosomes to chromatin domains several Mb long. Post-translational modifications (PTM) of core histones seem to be involved in chromatin structural transitions, but how remains unclear. To explore this, we used ChIP-seq and two cell types, HeLa and lymphoblastoid (LCL), to define how changes in chromatin packaging through the cell cycle influence the distributions of three transcription-associated histone modifications, H3K9ac, H3K4me3 and H3K27me3. We show that chromosome regions (bands) of 10–50 Mb, detectable by immunofluorescence microscopy of metaphase (M) chromosomes, are also present in G<sub>1</sub> and G<sub>2</sub>. They comprise 1–5 Mb sub-bands that differ between HeLa and LCL but remain consistent through the cell cycle. The same sub-bands are defined by H3K9ac and H3K4me3, while H3K27me3 spreads more widely. We found little change between cell cycle phases, whether compared by 5 Kb rolling windows or when analysis was restricted to functional elements such as transcription start sites and topologically associating domains. Only a small number of genes showed cell-cycle related changes: at genes encoding proteins involved in mitosis, H3K9 became highly acetylated in G<sub>2</sub>M, possibly because of ongoing transcription. In conclusion, modified histone isoforms H3K9ac, H3K4me3 and H3K27me3 exhibit a characteristic genomic distribution at resolutions of 1 Mb and below that differs between HeLa and lymphoblastoid cells but remains remarkably consistent through the cell cycle. We suggest that this cell-type-specific chromosomal bar-code is part of a homeostatic mechanism by which cells retain their characteristic gene expression patterns, and hence their identity, through multiple mitoses.

Post-translational modifications (PTM) of histone proteins have been closely linked to control of gene expression at multiple levels. Modifications, singly or in combination, often act by providing binding sites through which regulatory proteins can be targeted to specific regions of the genome, thus allowing regulation of genes or groups of genes<sup>1</sup>. This process can operate at a local level through a promoter or other relatively small region (several Kb) but can also bring about more widespread changes in packaging. For example, some modifications, such as H3 acetylated at lysine 9 (H3K9ac) and H3 trimethylated at lysine 4 (H3K4me3) both show sharply defined peaks at the promoters and TSS of active and potentially active genes<sup>2</sup>, while mono-methylated H3K4 is specifically enriched at enhancers<sup>3</sup>. Other modifications mark silent regions, including highly condensed facultative and centric heterochromatin (H3K27me3 and H4K20me3 respectively), and are generally much more widely spread, in some cases covering several Mb<sup>4,5</sup>. In most cases the structural and functional mechanisms that underpin these associations are still incompletely understood.

Recently, attention has been drawn to the ability of chromatin to undergo liquid–liquid phase transitions (LLPS<sup>6</sup>), a physical shift with the potential to bring about increased chromatin compaction over large genomic regions<sup>7–10</sup>. At the same time, transcriptionally active chromatin has been shown to form condensates via transcriptional coactivators and RNA pol II phosphorylation<sup>11–13</sup>. Intriguingly, at least in model systems, histone

<sup>1</sup>Chromatin and Gene Regulation Group, Institute of Cancer and Genomic Sciences, University of Birmingham, Birmingham B15 2TT, UK. <sup>2</sup>Bioinformatics, The Babraham Institute, Cambridge, UK. <sup>3</sup>Barts Cancer Institute, Queen Mary University of London, London, UK. <sup>4</sup>Epigenetics Programme, The Babraham Institute, Cambridge, UK. ✉email: j.halsall@bham.ac.uk; b.m.turner@bham.ac.uk

acetylation levels along with acetylation-binding bromodomain proteins, can be used to regulate LLPS<sup>14</sup>. The overall reduction in net change brought about by lysine acetylation is also likely to be influential.

Progression through the cell cycle provides a challenge for maintenance of patterns of transcription, particularly with respect to the dramatic changes in chromatin compaction that accompany passage through mitosis. Chromosome condensation leading up to metaphase disrupts the 3D organisation of the genome, with implications for the retention of cell-specific gene expression patterns. For example, interphase chromosomes are organised into topologically associating domains (TADs). These large, self-interacting chromosome regions bring together genes and genomic elements and are closely involved in their regulation<sup>15,16</sup>. Histone modifications mark or are confined by TADS, showing similar distribution within individual domains but significant differences between neighbouring domains<sup>17</sup>. But TADs are undetectable in mitotic chromosomes<sup>18</sup>, raising the question of how their cell-type-specific regulatory properties are conserved. Mitotic chromatin condensation is also associated with, and may sometimes be responsible for, the expulsion of some transcription factors from mitotic chromatin<sup>19</sup>. Others, sometimes referred to as bookmarking factors, are selectively retained<sup>20</sup>. A recent comprehensive proteomic analysis has suggested that only a minority of transcription factors found on chromatin were depleted during mitosis and the regulatory landscape remained relatively unchanged<sup>21</sup>.

Maintenance of histone PTM levels and distribution through the cell cycle is complex, both because different PTM are maintained as a dynamic steady-state balance through the actions of different modifying and demodifying enzymes, and because newly assembled chromatin at S-phase must somehow re-establish regional modification patterns. Histone modifications carried on the parental histones are diluted into newly formed chromatin and it is thought they act as template to reinstate chromatin marking to pre-replication levels<sup>22</sup>. This happens at different rates for different modifications. Most modifications, including acetylation, are reinstated rapidly by the modification of new histones within a single cell cycle. However, the propagation of heterochromatic marks H3K27me3 and H3K9me3 on new histones takes longer than a cell cycle, requiring ongoing modification of old and new histones to maintain modification levels<sup>23</sup>.

Overall levels of some histone PTM change rapidly as cells prepare to enter, or leave, mitosis. For example, histone H3 phosphorylation at serine 10 (H3S10ph) is dramatically increased during mitosis and seems to be essential for the compaction of chromatin required for cell division<sup>24–26</sup>. Phosphorylation of serine 28<sup>27</sup> and threonine 3<sup>28</sup> is also enriched in mitosis. It is interesting that all three phosphorylatable serines are adjacent to lysines whose modifications play critical roles in gene expression<sup>29</sup>.

Histone acetylation levels are reduced during mitosis<sup>21,30</sup>, and this deacetylation seems to be required for accurate chromatin segregation<sup>31</sup>. Nevertheless, we and others have shown that metaphase chromosomes contain readily detectable levels of the acetylated isoforms of all four core histones<sup>30,32</sup> and Ginno et al. showed relatively little change in chromatin accessibility (by ATAC-seq) even in mitotic chromatin<sup>21</sup>. Further, PTM associated with regulation of transcription (such as H3K9ac, H3K4me3, H3K27me3) are depleted in centromeric regions<sup>30</sup> but have characteristic and overlapping distributions (bands) across chromosome arms<sup>32</sup>. These bands range in size from 10 to 50 Mb and correspond to more gene-rich regions of the genome<sup>32–34</sup>. These PTM serve as markers for such regions through mitosis.

Here we use cell cycle sorting and ChIP-seq to analyse the genomic distribution of three histone modifications closely associated with transcriptional regulation (H3K9ac, H3K4me3 and H3K27me3) through the cell cycle in two human cell types. Reconstituting these data at pseudo-microscopic resolution we demonstrate that the banding patterns visible in mitotic chromosomes are remarkably strongly conserved from G<sub>1</sub> to G<sub>2</sub>M and correlate with the patterns observed by metaphase chromosome staining. At higher (< 5 Mb) resolution, the bands were made up of clearly defined sub-bands that differed between cell-types. Remarkably, these patterns remained consistent through the cell cycle. At the individual gene level, we have identified a small number of local, cell-cycle-dependent changes within this stable, cell-specific landscape. These mark genes with mitosis-specific functions, whose selective transcription persists into G<sub>2</sub>M.

## Results

Human lymphoblastoid cells (LCL, diploid, non-cancerous) and HeLa cells (aneuploid, cancer-derived) were fractionated into cell cycle phases (G<sub>1</sub>, G<sub>2</sub>M and M) by either flow cytometry (based on DNA content), centrifugal elutriation (largely based on size) or mitotic shake off (applicable only to HeLa). Details of cell culture conditions, fractionation techniques and the purity of isolated fractions are presented in “Methods” and Supplementary Fig. S1. Lymphoblastoid cells are an Epstein-Barr virus immortalised B cell line. Despite being immortal and thus a convenient cell culture model, they are pre-malignant, karyotypically normal and formed the basis of our earlier studies of histone modification patterns in metaphase cells<sup>32</sup>. HeLa cells are a much-studied cervical cancer cell line. They are aneuploid, but offer the advantage that upon mitotic shakeoff they yield very highly enriched metaphase populations (Supplementary Fig. S1). Overall, based on DNA content and microscopy, G<sub>1</sub> fractions were 80–90% pure, G<sub>2</sub>M fractions were 70–90% pure and mitotic shake off fractions were almost 100% pure. G<sub>2</sub>M fractions were > 90% G<sub>2</sub> (i.e. < 10% M).

Fractionated cells were fixed in acetone prior to preparation of chromatin by micrococcal nuclease digestion. This revised procedure rapidly inactivates enzymes that might disrupt histone modifications during in-vitro processing while allowing efficient chromatin digestion to give nucleosomal fragments. We found no significant differences in chromatin yield or fragment size between different cell cycle fractions (Supplementary Fig. S1E).

Chromatin was immunoprecipitated with rabbit polyclonal antisera to two histone modifications associated with transcriptionally active chromatin, H3K4me3, H3K9ac and one modification associated with gene silencing and formation of facultative heterochromatin, H3K27me3. Overall, ChIP-seq data obtained using our protocol for LCL cells correlate closely with results for the same cell type available through ENCODE (Supplementary Fig. S2).

**Bands of histone PTM detected by immunofluorescence microscopy on metaphase chromosomes are also present in interphase and are made up of smaller sub-bands.** To define the regional distribution of the chosen modifications, ChIP-seq data were quantified using rolling windows and visualised using a red-green colour scale, mimicking metaphase chromosome staining by immunofluorescence (IF) (see “Methods” for details). These interphase chromosomes assembled from ChIP-seq data were aligned with the corresponding chromosome from LCL metaphase chromosome spreads, immunolabelled with antisera to H3K9ac, H3K4me3 and H3K27me3.

Presented in this way, H3K9ac and H3K4me3 show very similar banded distributions along chromosomes, with interspersed regions of relatively high (green) and low (red) modification (Fig. 1A, complete ChIP-seq karyotypes in Supplementary Figs. S3 and S4). In the images shown, the pixel resolution (i.e. minimum visible band size), is approximately 1.5 Mb. Large regions (10–50 Mb) relatively rich in modified histone and corresponding to bands detected by IF<sup>32</sup> were identifiable in interphase chromosomes as clusters of smaller (1–5 Mb), enriched (green) bands. (Chromosomes 1, 3, 6 and 12 provide particularly clear examples, Fig. 1).

The polycomb-associated modification H3K27me3 was more widely distributed across interphase chromosomes, consistent with the more diffuse banding pattern revealed by immunofluorescence microscopy of metaphase chromosomes<sup>32</sup>. As with the “active” modifications, immunofluorescent H3K27me3 bands detected in metaphase chromosomes were present in interphase and comprised multiple, smaller sub-bands (Fig. 1A, full karyotype in Supplementary Fig. S5).

**Chromosome sub-bands defined by histone PTM differ between cell types but are largely unchanged through the cell cycle.** At microscopic (10–50 Mb) resolution, there were strong similarities in banding patterns between LCL and HeLa, but clear differences in the distribution of sub-bands were visible (Fig. 1B, Supplementary Fig. S3).

This is consistent with the conservation of IF banding patterns in LCL and primary lymphocytes<sup>32,35</sup> and with IF staining of a human x mouse somatic cell hybrid containing only human chromosome 11. The chromosome retained its characteristic banding pattern when immunostained with antibodies to H3K4me3, despite being housed in a foreign (mouse) cellular environment (Supplementary Fig. S6).

Visually, the distributions show only very minor differences between G<sub>1</sub> and G<sub>2</sub>M chromosomes in LCL (Figs. 1A, Fig. S3A, Fig. S4, Fig. S5) and G<sub>1</sub>, G<sub>2</sub>M and metaphase chromosomes (M) in HeLa (Figs. 1B, Fig. S3B). Thus, in each cell type, every chromosome has its own distinctive and cell-type-specific pattern of bands and sub-bands. This pattern changes very little through the cell cycle, including metaphase.

These results all suggest that, at microscopic resolution (10–50 Mb), histone modification patterns are dependent primarily on genomic features embedded in DNA sequence, such as gene density or frequency of repetitive elements<sup>32</sup>. At higher resolution (1–5 Mb), cell-type-specific differences are revealed that may reflect, or even determine, inter-cellular differences in gene expression pattern.

**Correlation analysis at <1 Mb resolution confirms the stability of histone modification patterns through the cell cycle.** To obtain an unbiased estimate at sub-Mb resolution of genome-wide changes in histone PTM through the cell cycle, we used a rolling window analysis of our ChIP-seq data. For such analysis, the choice of window size is crucial. To examine this, we scanned our ChIP-seq data using a series of rolling windows from 1 Mb to 100 bp. For each window size, we calculated the correlation (Pearson R value) between cell cycle phases for H3K4me3, H3K9ac and H3K27me3. R values (R) were plotted against window size (W). Figure 2A shows R v window size (W) for H3K4me3, H3K9ac and H3K27me3 for G<sub>1</sub> vs G<sub>2</sub>M in LCL (left), along with H3K9ac for G<sub>1</sub> vs G<sub>2</sub>M, G<sub>1</sub> v M and G<sub>2</sub>M vs M in HeLa cells (right).

In all cases, R was very high (>0.99) for window sizes above 50 Kb. There was then an elbow at 5–10 Kb below which R fell more rapidly, dropping to between 0.6 and 0.8 at a window size of 100 bp. It seems that histone modification patterns are extremely well conserved through the cell cycle, even at resolutions approaching the size of a single nucleosome (200 bp, Fig. 2A).

While the reduced value of R at window sizes below 5–10 kb could be due to differences in the regional distribution (micro-banding) of histone PTM, it more likely reflects a growing number of windows containing very few or no reads at low window sizes. This inevitably leads to increased variance. In Supplementary Fig. S7, we show that simply reducing the number of reads in the dataset progressively shifts the inflexion point (elbow) to higher values of W.

Based on these results, we selected a window size of 5 Kb for further analyses. It is large enough to avoid inaccuracies caused by low integer read counts but not so large that any regions of difference between samples are lost within larger unchanging regions. Using 5 Kb windows, there is a strong correlation for all modifications studied between G<sub>1</sub> and G<sub>2</sub>M phases in LCL (R=0.907–0.94, Fig. 2B) and G<sub>1</sub>, G<sub>2</sub>M and M phases in HeLa (R=0.957–0.976, Fig. 2C).

Although genomic elements including enhancers, promoters and centric heterochromatin, are often identifiable by their exceptional levels of individual histone modifications, the identification of functionally distinct sub-categories often requires analysis of combinations of histone PTM (see<sup>36</sup> for examples). A particularly striking example is provided by the regions designated bivalent domains that are enriched in *both* activating and silencing histone PTM (H3K4me3 and H3K27me3 respectively) and are prominent in both mouse<sup>37</sup> and human<sup>38–40</sup> embryonic stem cells. This unusual combination of PTM marks a chromatin state in which genes, required for progression down specific developmental pathways, are poised to become active when the appropriate developmental signals are received.

We used scatter plots constructed from 5 kb windows centred on transcription start sites (TSS) to compare levels of H3K4me3 and H3K27me3 in G<sub>1</sub> and G<sub>2</sub>M human LCL (Fig. 2D). This revealed three distinct populations, representing TSS unmarked by either modification (9995 unique genes), TSS high in H3K4me3 and

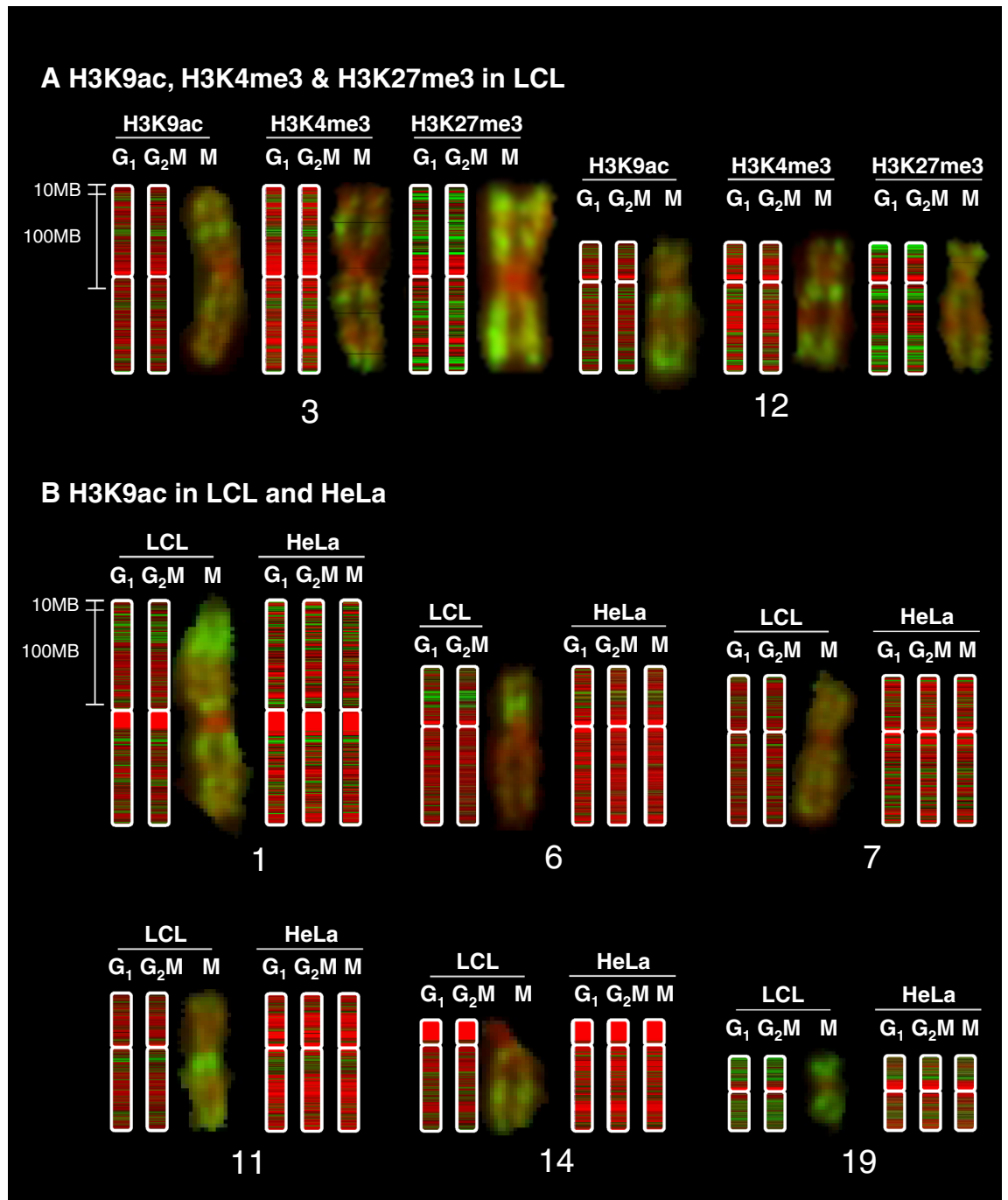


**Figure 1.** Metaphase chromosome banding patterns are conserved through the cell cycle but differ between cell types. ChIP-seq data were analysed using rolling windows and displayed as blocks using a red-green colour scale in SeqMonk. A scale bar is shown, and as a rough guide, the blocks of centric heterochromatin (uniform red) at chr1q1 are 20 Mb in size. Maximum resolution (1 pixel) is approximately 1.5 MB. G<sub>1</sub> and G<sub>2</sub>/M fractions were sorted by FACS (LCL) or centrifugal elutriation (HeLa). Mitotic HeLa cells were harvested by mitotic shake-off. LCL ChIP-seq karyotypes in G<sub>1</sub> and G<sub>2</sub>/M are shown aligned with metaphase chromosomes stained with antibodies to H3K9ac, H3K4me3 and H3K27me3 as described previously<sup>32</sup> (A). H3K9ac karyotypes in G<sub>1</sub>, G<sub>2</sub>/M and M are shown in LCL and HeLa cells (B).

low in H3K27me3 (10,156 genes) and those low in H3K4me3 and high in H3K27me3 (8315 genes). In these differentiated cells only a small proportion of genes (2825 genes) were present in bivalent domains, relatively highly enriched in both marks. This pattern was consistent between cell cycle phases and TSS retained their position in the distribution from G<sub>1</sub> to G<sub>2</sub>/M (Fig. 2D, insets). Expression levels from genes in each population were determined by microarray from asynchronous cells (Fig. 2E). Functional enrichment of genes from each quadrant is summarised in Supplementary figure S8. As might be expected, expression was highest from TSS with

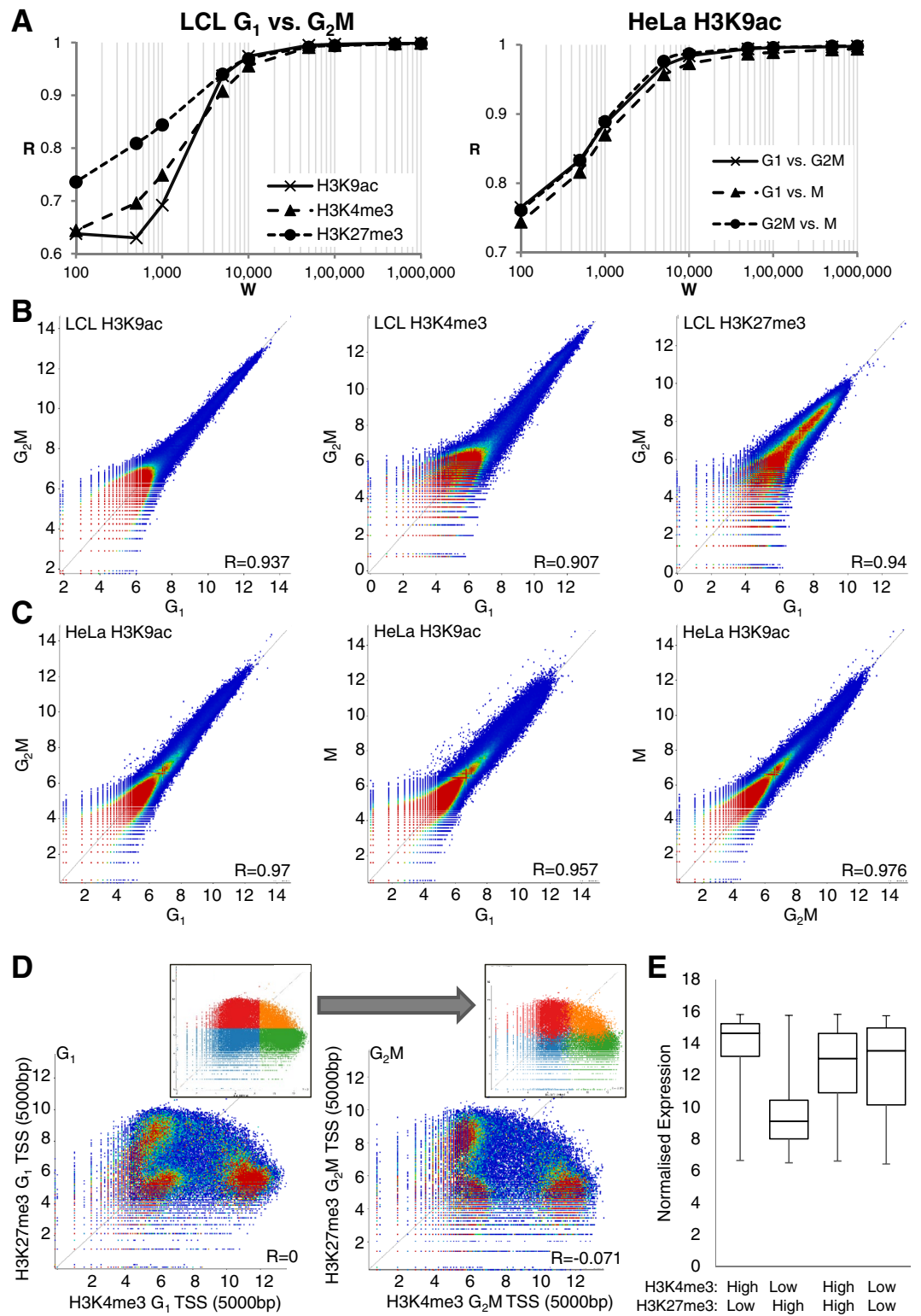


**Figure 2.** Rolling window analysis of histone modification patterns shows strong conservation through the cell cycle. **(A)** ChIP-seq of H3K9ac, H3K4me3 and H3K27me3 were compared in  $G_1$  vs.  $G_2M$  in LCL and H3K9ac in  $G_1$  vs.  $G_2M$  vs. M in HeLa cells using rolling windows of various sizes. Pearson correlation coefficient R is plotted against window size (W) for rolling windows of 100 bp–1 MB. **(B)** 5 kb windows were subsequently chosen as most informative and rolling window comparison of H3K9ac, H3K4me3 and H3K27me3 in  $G_1$  vs.  $G_2M$  by dotplot is shown in FACS-sorted LCL and **(C)** elutriation and mitotic shake-off sorted HeLa cells. Values represent  $\log_2$  read count normalised to total read count in a 5 kb rolling window analysis with a 5 kb step. Pearson R values for each correlation are indicated. **(D)** Using 5 kb windows centred on transcription start sites (TSS), H3K4me3 was plotted against H3K27me3 in LCL in  $G_1$  and  $G_2M$ . Insets show the division of the  $G_1$  plot into quadrants and the subsequent position of these probes in the  $G_2M$  plot. **(E)** Expression levels of genes from TSS in each quadrant were measured by microarray and summarised by boxplot showing median, interquartile range, minimum and maximum.

high H3K4me3 and low H3K27me3 and this group was modestly enriched in genes involved in housekeeping processes such as mitochondria (fold enrichment (FE) 1.7,  $P = 2.5 \times 10^{-18}$ ), ribonucleoprotein complex (FE 1.9,  $P = 9.6 \times 10^{-14}$ ) and RNA processing (FE 1.7,  $P = 1.6 \times 10^{-9}$ ). Expression was lowest from TSS with high H3K27me3 and low H3K4me3 and these genes were enriched in cell-type specific genes which would not be expected to be expressed in LCLs such as epidermis development (FE 2.2,  $P = 8.5 \times 10^{-8}$ ), neurological system process (FE 1.5,  $P = 2.7 \times 10^{-12}$ ) and embryonic organ morphogenesis (FE 2.1,  $P = 1.2 \times 10^{-5}$ ). Genes with high levels of H3K4me3 and H3K27me3 or low levels of both marks at their TSS showed a broader range of expression, suggesting these two marks were not sufficient to define their transcriptional status. Despite LCLs being differentiated cells, Hox genes were enriched within the H3K4me3 high, H3K27me3 high “bivalent” group of TSS (FE 3.1,  $P = 0.003$ ). It has been shown that in human ES cells, the level of H3K4me3 at bivalent promoters varies through the cell cycle, with some genes showing elevated H3K4me3 exclusively at mitosis. Intriguingly, these genes showed the strongest up-regulation after induction of differentiation. Further, in differentiated cells, levels of H3K4me3 at bivalent domains became stable through the cell cycle<sup>40</sup>, a finding consistent with our results in LCL. In differentiated cells, it was shown that the writers of active modifications generally dissociate from mitotic chromatin while writers of silencing marks, including members of the polycomb complex are retained<sup>21</sup>.

**Differences in H3K9ac distribution between cell types reflect cell-type-specific transcription.** When H3K9ac modification patterns were compared between HeLa and LCL, correlation was lower than between cell cycle phases, though still high overall ( $G_1$   $P = 0.781$ , Fig. 3A,  $G_2M$   $P = 0.808$ , not shown). A small number (~6%) of windows showed greater difference, with relatively high modification levels in HeLa or LCL, indicative of cell-specific PTM levels. To explore this further, the 3% of windows exhibiting the highest differential enrichment in H3K9ac in HeLa relative to LCL and, conversely, the 3% of windows most enriched in H3K9ac in LCL relative to HeLa, were selected and the associated genes extracted. These outlying windows were relatively gene dense (27 genes/Mb for the LCL > HeLa group, 57 genes/Mb for the HeLa > LCL group, compared with 14.1 genes/Mb for the whole genome). Expression levels from genes within these regions were analysed by microarray, revealing that H3K9ac enrichment correlated with gene expression: those probes most enriched in H3K9ac in LCL compared to HeLa contained genes more highly expressed in LCL and vice versa (Fig. 3B). Ontology analysis is summarised in Fig. 3C and revealed that windows more enriched in H3K9ac in LCL than HeLa cells contained genes involved in B-cell receptor signalling pathway (FE 5.9,  $P = 3.6 \times 10^{-15}$ ), adaptive immune response (FE 2.9,  $P = 9.9 \times 10^{-9}$ ) and MHC class II protein complex (FE 5.3,  $P = 4.3 \times 10^{-5}$ ). In contrast, regions more H3K9ac-enriched in HeLa contained genes involved in cell–cell adhesion junction (FE 2.0,  $P = 9.4 \times 10^{-20}$ ) and pathways in cancer (FE 1.5,  $P = 9.9 \times 10^{-8}$ ), including oncogenes such as ERBB2, WNT5A and BRAF.

**Histone modification levels at topologically associated domains do not change through mitosis.** As a first step towards linking sub-microscopic histone PTM banding with genomic function, we examined histone modification levels within topologically associated domains, TADs<sup>15,16</sup>. These domains range in size from about 0.5 to 2 Mb, with a median size of around 0.9 Mb<sup>15</sup>. They show a characteristic distribution of histone modifications, including H3K4me3 and H3K27me3<sup>16</sup>, with boundary elements appearing to constrain the spread of heterochromatin<sup>15</sup>. TAD structure is lost as chromosomes condense during mitosis and re-emerges during early  $G_1$ <sup>18</sup>. We quantified ChIP-seq read counts within TADs using TAD coordinates defined in the ENCODE tier 1 LCL line GM12878 by Rao et al.<sup>16</sup> and in HeLa cells by Thiecke et al.<sup>41</sup> based on data from Wutz et al.<sup>42</sup>. We compared levels of H3K4me3, H3K9ac and H3K27me3 in  $G_1$  vs  $G_2M$  in LCL, and H3K9ac in  $G_1$  vs  $G_2M$  vs M in HeLa cells. We found that histone modification levels within TADs were strongly conserved from  $G_1$  into  $G_2M$  and M in both LCL ( $R = 0.982$ – $0.993$ , Fig. 4A) and HeLa ( $R = 0.968$ – $0.991$ , Fig. 4B). As might be expected, the lowest correlation was between  $G_1$  and M and the highest between  $G_2M$  and M. As shown in Fig. 4C, distribution of histone PTM across TADs, particularly that of H3K27me3, appears to be confined by the subcompartment boundaries defined by Rao et al.<sup>16</sup>. However there was no reduction in signal or redistribution from  $G_1$  into  $G_2M$  and M, despite the disappearance of detectable TADs in metaphase<sup>18</sup>.

TADs contain more than a single gene, and these can be active, inactive or a mixture of both. Similarly, most TADs contain a mixture of “activating” (H3K9ac, H3K4me3) and “silencing” (H3K27me3) histone modifications, the former distributed as sharp peaks (< 5 Kb), marking DNA elements such as promoters or enhancers and the latter as broader genomic regions, sometimes incorporating several control elements or coding regions. This is all consistent with previous data<sup>4,36,43</sup>, but what is remarkable is the strict, general conservation of these distributions through the cell cycle, despite the structural reorganization involved. Our results raise the interesting possibility that a conserved pattern of histone modification facilitates the reassembly of TADs in a way that preserves their distinctive transcriptional properties.

**Gene function and expression timing modulate histone modification at specific transcription start sites.** We next focussed on the regulatory regions around transcription start sites (TSS). The average distribution of H3K4me3 across TSS showed a characteristic bimodal profile around TSS in LCL (Fig. 5A), with the expected nucleosome-free region<sup>44</sup> and the highest modification levels at the +1 nucleosome, decreasing over subsequent nucleosomes to basal levels by approximately 2000 bp into the gene body. The average distribution did not vary significantly between  $G_1$  and  $G_2M$ . We saw very similar average distributions around TSS for a second modification, H3K9ac (Fig. 5C). Using TSS windows from – 500 bp to + 750 bp, approximately incorporating the first nucleosome upstream of the nucleosome free region (– 1) and the first three downstream nucleosomes (+ 1 to + 3), we showed that H3K4me3 and H3K9ac levels at TSS correlated very strongly between  $G_1$  and  $G_2M$  ( $R = 0.964$  and  $0.967$  respectively, Fig. 5B and D).

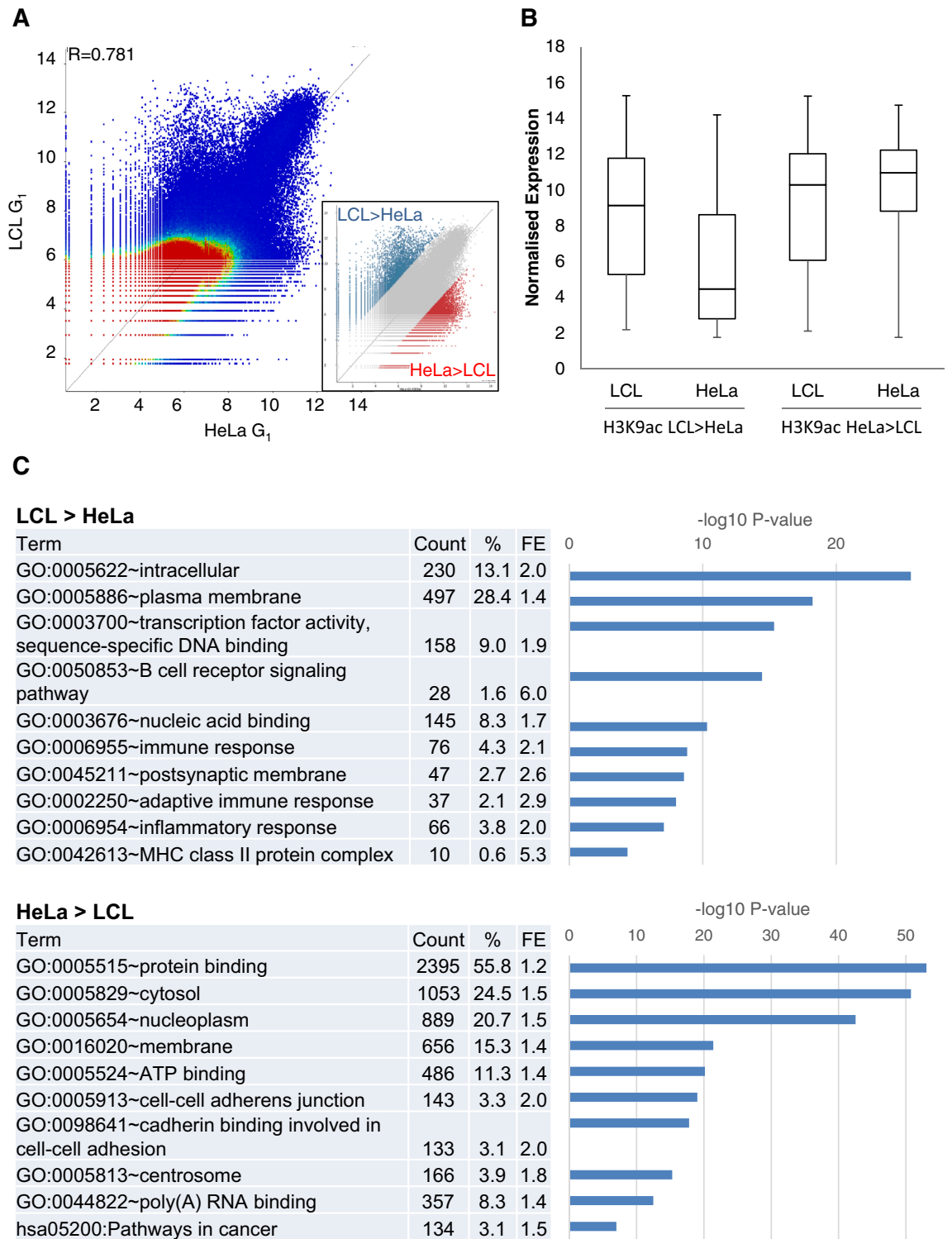


**Figure 3.** Differences in H3K9ac pattern between LCL and HeLa reflect cell-type-specific transcription. **(A)** Dotplot comparison of H3K9ac in 5 kb windows between LCL and HeLa in G<sub>1</sub>. The outlying 3% on each side of the distribution are highlighted (inset). **(B)** The expression of genes contained within these outlying regions was measured by microarray in LCL and HeLa. **(C)** Ontology analysis for functional enrichment was carried out on genes in each outlying region using DAVID. Count: number of significant genes with specific annotation; %: proportion of genes in each gene list with specific annotation; FE: Fold enrichment.

Despite the strong correlations shown by these scatter plots, there are outliers towards the edges of the distributions (Fig. 5). We asked whether these have any functional significance, perhaps representing distinct

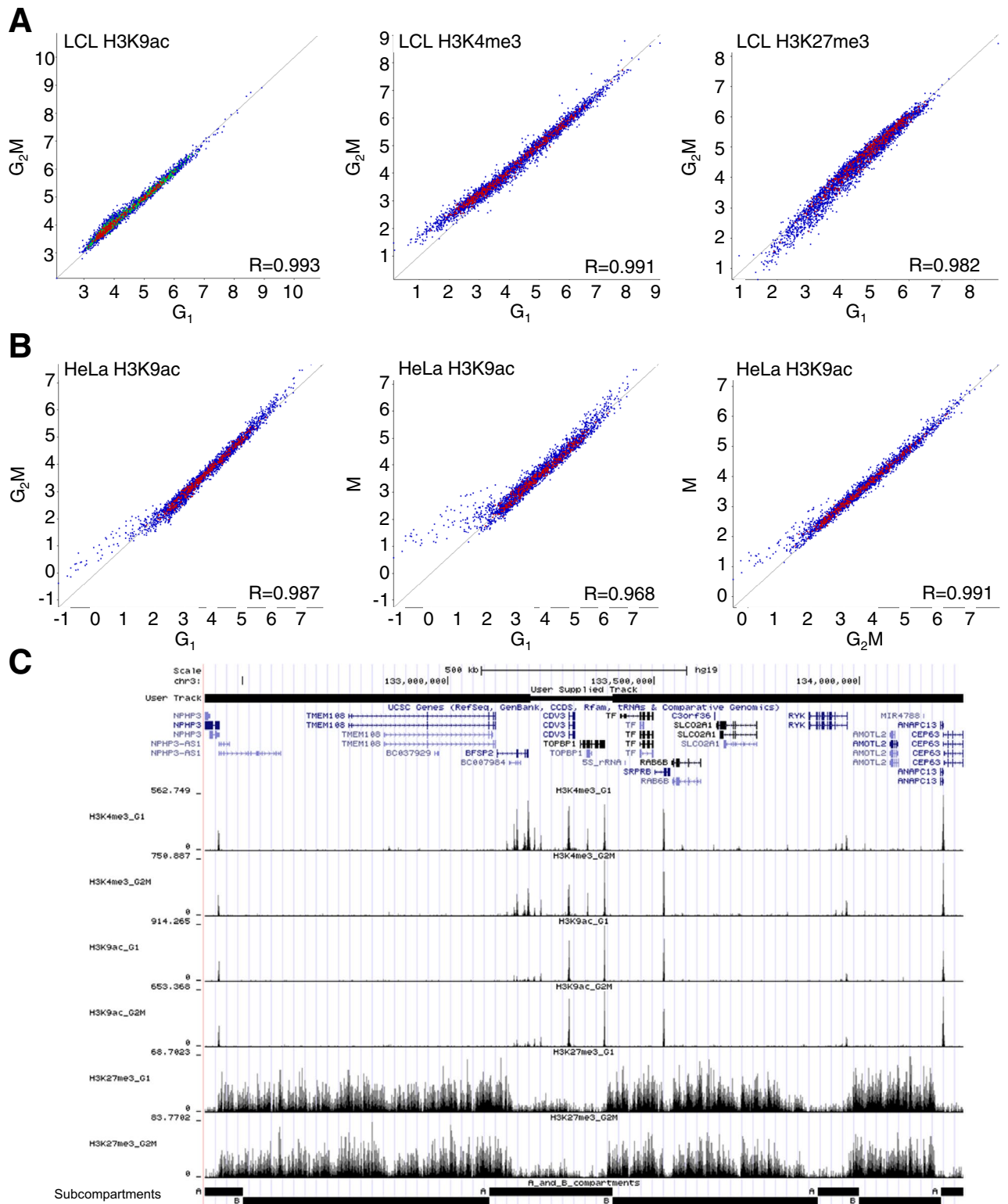


**Figure 4.** Histone modification levels are conserved within topological domains throughout the cell cycle. **(A)** Comparison of H3K9ac, H3K4me3 and H3K27me3 in  $G_1$  vs.  $G_2M$  in FACs-sorted LCL and **(B)** H3K9ac in HeLa in  $G_1$  vs.  $G_2M$ ,  $G_1$  vs. M and  $G_2M$  vs M (elutriated/MSO). Topological domain coordinates from Rao et al.<sup>16</sup> (LCL) and Thiecke et al.<sup>41</sup> (HeLa) were used to define probes. Values represent  $\log_2$  read count normalised to total read count, corrected for probe size. Pearson R values are given for each correlation. **(C)** A genome browser screenshot of cell-cycle specific ChIP-seq data on chromosome 3. All tracks are from LCL. Topological A and B domains defined in the GM12878 LCL line<sup>16</sup> are shown.

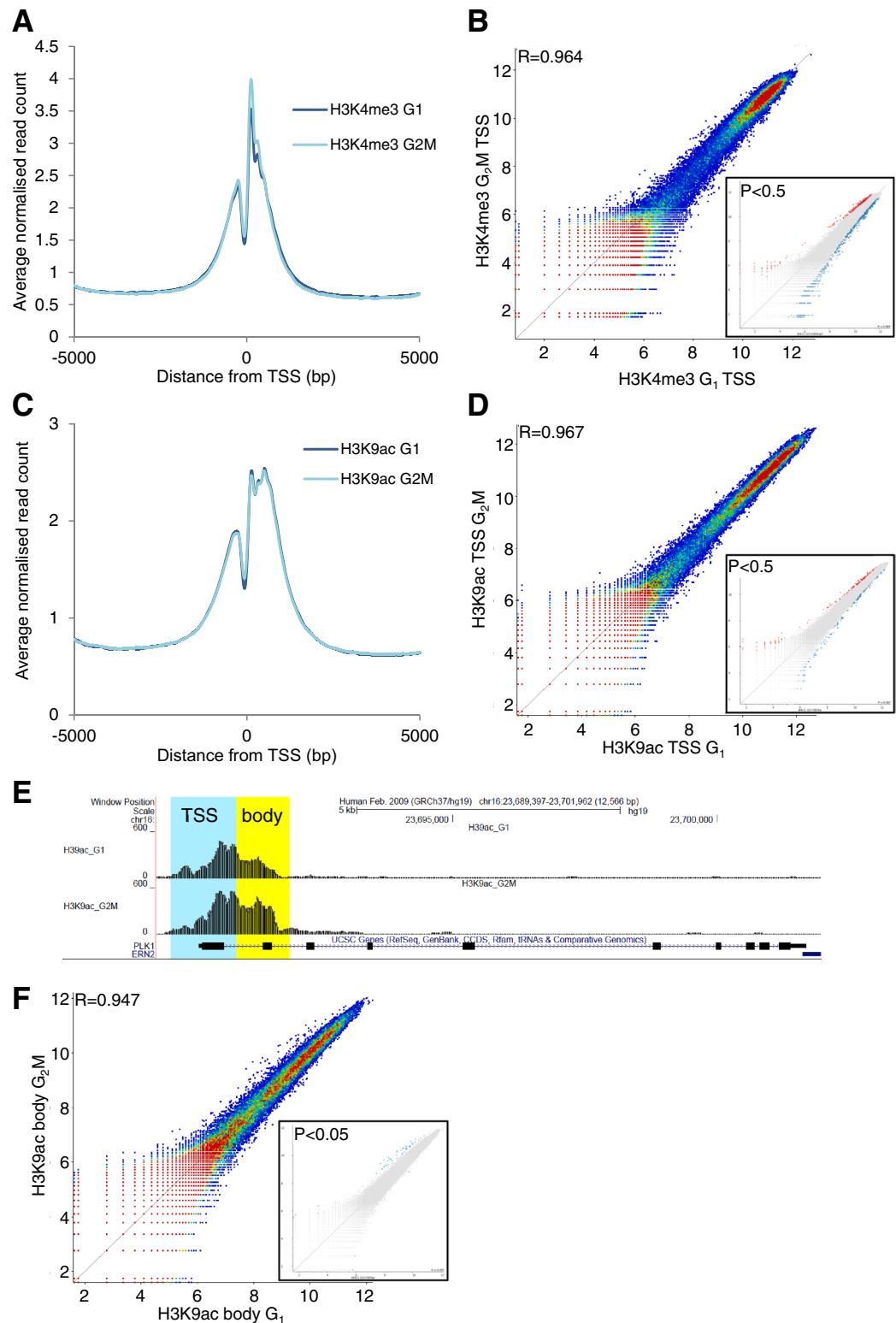


**Figure 5.** H3K4me3 and H3K9ac enrichment at transcription start sites is conserved in LCL, with outliers representing specific gene function. (A, C) Average distribution (average read count normalised to total read count) across a 10 kb window centred on all transcription start sites (TSS) for H3K4me3 (A) and H3K9ac (C) in G<sub>1</sub> and G<sub>2</sub>M in LCL. (B, D) Modification levels at the proximal TSS (− 500 to + 750 bp) are compared by dotplot for H3K4me3 (B) and H3K9ac (D). Outliers were selected by intensity difference ( $P<0.5$ , insets) for ontology analysis. (E) Extension of the H3K9ac signal further into the gene body (+ 750 to + 1750 bp) was observed for a few genes with function in mitosis, e.g. PLK1. (F) Comparison of H3K9ac enrichment in this region is shown and outliers highlighted ( $P<0.05$ , inset).

classes of genes. Intensity difference ( $P < 0.5$ ) was used to identify outliers (Fig. 5B, D, inset panels). These genes were subjected to ontology analysis using DAVID. Strikingly, gene populations selected for high levels of either H3K4me3 or H3K9ac in  $G_2M$  relative to  $G_1$ , were consistently and strongly enriched in GO terms related to mitosis (Supplementary Table S1, FE 2.3–10.4,  $P = 4 \times 10^{-11}$ –0.004). When TSS significantly enriched in H3K9ac in  $G_1$  or  $G_2M$  were highlighted on the H3K4me3 scatterplot (Supplementary Fig. S9A), they aligned to the same side of correlation and vice-versa (Supplementary Fig. S9B), showing that at higher, i.e. more accurate, levels of modification, the two PTM are closely correlated.

We also observed that at some TSS with H3K9ac enrichment in  $G_2M$ , modification levels extended further into the gene body in  $G_2M$  than in  $G_1$ . For example, this is shown for PLK1, the cell cycle regulating serine/threonine kinase whose expression peaks in mitosis<sup>45</sup> (Fig. 5E). We therefore correlated gene body (+750 bp to +1750 bp) acetylation levels (Fig. 5F) in  $G_1$  and  $G_2M$ . Correlation was again strong with a small group of outliers, which were statistically more significant ( $P < 0.05$ ) than those for TSS and were almost entirely enriched in  $G_2M$  relative to  $G_1$  (Fig. 5F, inset). This small group of genes was extremely strongly enriched in mitotic terms (Supplementary Table S1): genes annotated as involved in mitotic cell cycle comprised 10 of 26 genes enriched in the gene body in  $G_2M$ , representing a fold enrichment of 19.2 ( $P = 3.0 \times 10^{-10}$ ).

It may be that increased H3K9ac in  $G_2M$  is due to transcription, late in the cell cycle, of genes whose products are required for mitosis. To test this, we used centrifugal elutriation to isolate 4 fractions of lymphoblastoid cells at sequential points through the cell cycle (Fig. 6A). We then carried out RT-PCR using primers specific for the pre-mRNA of genes previously shown to have particularly high H3K9ac in  $G_2M$  (those genes that were outliers in Fig. 5F), spreading across the TSS and into the gene body. The results are shown in Fig. 6B. Of 7 genes with elevated H3K9ac in  $G_2M$ , transcript levels were always highest in fractions 3 and 4, consisting predominantly of  $G_2M$  cells. Conversely, a single gene (NBN) with comparably elevated H3K9ac in the gene body in  $G_1$  cells showed slightly elevated transcription in fractions 1 and 2 (Fig. 6B), containing a majority of  $G_1$  cells (Fig. 6B).

H3K9ac enrichment at TSS was also strongly conserved through the cell cycle, including metaphase, in HeLa cells, ( $G_1$  vs  $G_2M$ ,  $R = 0.978$ ;  $G_1$  vs M,  $R = 0.967$ ;  $G_2M$  vs M,  $R = 0.975$ , Fig. 7). When minor outliers at the edges of the correlation were identified ( $P = 0.5$ , Fig. 7B, inset panels), mitotic terms were again over-represented in TSS enriched in  $G_2M$  and M relative to  $G_1$  (FE = 3.0 and 1.6,  $P = 0.004$  and  $P = 0.003$  respectively, Fig. 7, Supplementary Table S2).

Thus, increased histone acetylation is closely linked to the selective expression of a group of genes necessary for mitosis at the appropriate stage of the cell cycle. The change in acetylation occurs in the same cell cycle phase ( $G_2$ ) as the increase in transcription, suggesting that it is part of the transcription process rather than a pre-determining marker of selected genes. A more detailed temporal analysis of the two events will be necessary to resolve this.

In HeLa, but not LCL, translational terms, particularly ribosomal protein genes, were strongly enriched in H3K9ac in  $G_2M$  relative to  $G_1$  (FE 18,  $P = 1.1 \times 10^{-21}$ ). Surprisingly, large and small ribosomal protein genes (RPL and RPS) were further enriched in H3K9ac in M phase relative to  $G_2M$  (Supplementary Table S3), suggesting that differential marking is maintained through mitosis. Large and small ribosomal genes (28 of each) were all enriched in M relative to  $G_2M$  (FE 5.7 and 5.4,  $P = 2.2 \times 10^{-14}$  and  $1.4 \times 10^{-13}$  respectively, Supplementary Table S2). The position of RPL and RPS genes in the correlation scatterplots are shown in Fig. 7D, showing a strong bias towards enrichment in mitosis. M phase enrichment is also accompanied by a change in the average modification profile with a reduction in H3K9ac enrichment at the  $-1$  and  $+1$  nucleosomes from  $G_1$  to  $G_2M$  to M and higher enrichment further into the gene body (Fig. 7C), perhaps reflecting ongoing transcription of RP genes.

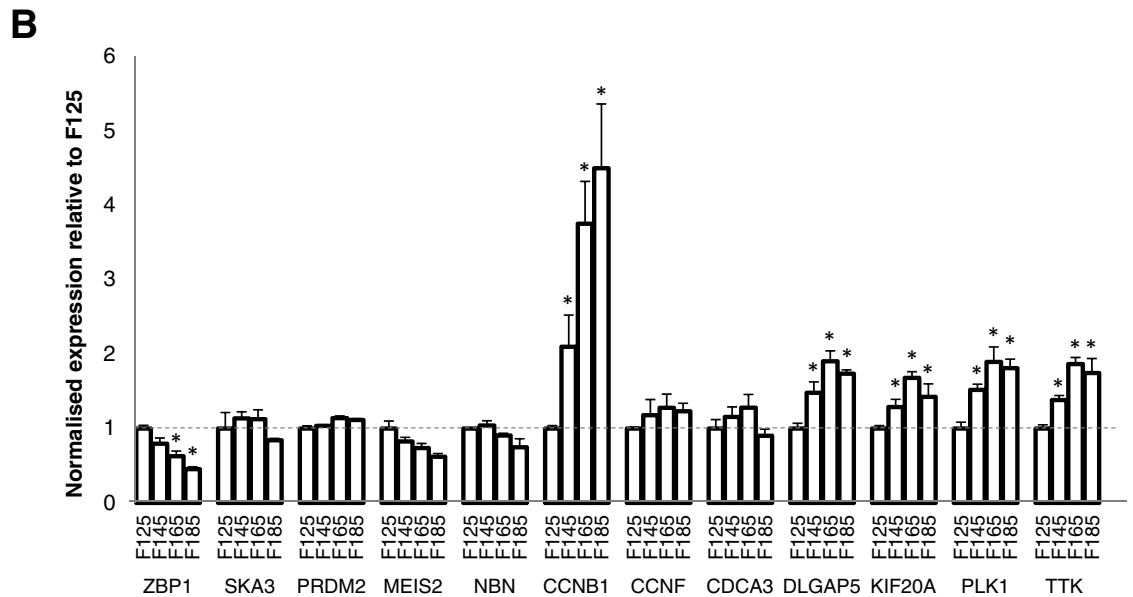
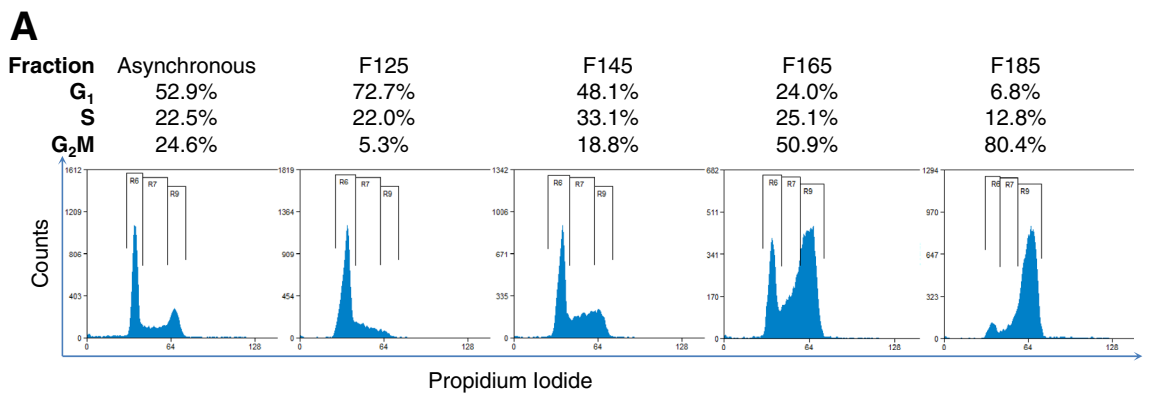
The H3K9ac around the TSS of RP genes extends further into the gene body, at all stages of the cell cycle, than TSS in general (all probes). In view of the results with mitosis-related genes preferentially transcribed in  $G_2$ , this suggests that RP genes may be transcribed throughout the cell cycle, including through mitosis. Whether transcription itself persists or not, the finding that levels of H3K9ac at RP gene TSS are higher in metaphase than any other stage of the cell cycle, suggests a chromatin mark that helps maintain the continuity of RP gene transcription through mitosis. Continued transcription is also consistent with our failure to detect any increase in RP transcript levels (compared to genes in general) as HeLa cells emerged from mitosis into  $G_1$ .

## Discussion

### Histone PTM, chromatin organisation and maintenance of cellular identity through the cell cycle.

Chromatin controls transcription in eukaryotes at multiple levels, from nucleosome packaging (repeat length of around 200 bp), to chromatin loops (exemplified by TADs, between 0.2 and 1.5 Mb) and various sub-nuclear structures visible at the light microscope level, such as blocks of centric heterochromatin, Polycomb bodies and nuclear speckles<sup>46–50</sup>. Structures can be built by chromatin looping mediated by protein–protein and protein–DNA binding<sup>51,52</sup> and by the spontaneous collapse of large chromatin domains at high concentration, leading to phase transitions and highly condensed blocks of chromatin<sup>6,53</sup>. Phase separation can be influenced by DNA sequence<sup>54</sup>, by overall levels of histone acetylation and bromodomain binding proteins<sup>14</sup> and by DNA methylation<sup>55</sup>, the latter two providing potentially mechanistic links between higher-order chromatin structures and common epigenetic marks. These structures influence transcription in various ways; they can restrict access of TFs and other functional proteins to their binding sites, and bring regulatory DNA elements (such as enhancers and promoters) into spatial proximity<sup>56</sup>. A key point for the present discussion is that these structures are all dynamic<sup>57</sup> and subject to disruption through the cell cycle; TADs and other higher order structures often disappear altogether through mitosis<sup>57,58</sup>. How then are cell-type-specific patterns of gene expression to be maintained?

To explore in more detail the link between histone PTM levels and transcription through the cell cycle, we scanned histone PTM across LCL and HeLa genomes using rolling 5 Kb windows. On scatter plots, a consistently



Mark	H3K4me3				H3K9ac							
Region	TSS (-500 - +750)				Gene body (+750 - +1750)							
Enriched Phase	G <sub>1</sub>	G <sub>2</sub> M	G <sub>1</sub>	G <sub>2</sub> M	G <sub>1</sub>	G <sub>2</sub> M						

**Figure 6.** H3K9ac gene body enrichment in G<sub>2</sub>M in LCL is associated with ongoing transcription. **(A)** LCL were fractionated by centrifugal elutriation. Elutriated fractions were fixed and stained with propidium iodide to determine cell cycle stage. The proportion of cells in G<sub>1</sub>, S and G<sub>2</sub>M for each elutriated fraction is shown above each plot. **(B)** Cell-cycle specific expression of genes with significant TSS enrichment was measured by RT-qPCR with primers to nascent pre-mRNA, normalised to the housekeepers β-actin, beta-2-microglobulin, RPL13A and HPRT. Genes were enriched in H3K4me3 at the TSS in G<sub>1</sub> (ZBP1) or G<sub>2</sub>M (SKA3), H3K9ac at the TSS in G<sub>1</sub> (PRDM2) or G<sub>2</sub>M (MEIS2) or in the gene body (+750–+1750) in G<sub>1</sub> (NBN) or G<sub>2</sub>M (all remaining genes). \*P < 0.05 relative to F125.

close correlation was found when different cell cycle phases were compared (R values between 0.91 and 0.98 for all three modifications). When the same procedure was used to compare H3K9ac at equivalent cell cycle phases in HeLa and LCL, the correlation, though still present, was much lower (R = 0.78). Further, outlying regions on either the LCL or HeLa sides of the distribution, were enriched in genes likely to be preferentially expressed in either HeLa or LCL, i.e. cell-type-specific genes. These results are consistent with the proposition that variation in PTM distribution at 1–2 Mb and below reflects the distinctive patterns of transcription, or transcriptional potential, that characterize the two cell types, LCL and HeLa.

Levels of histone PTM at transcription start sites, are even more highly correlated across the cell cycle than levels within unselected windows (R = 0.964 and 0.978). It seems that modification levels at TSS are almost invariant through the cell cycle. However, we identified a small group of genes with relatively high levels of H3K9ac and H3K4me3 across their TSS in G<sub>2</sub>M. Ontology analysis showed this group to be highly enriched in genes whose products are required for mitosis. We showed that primary transcript levels of selected members of

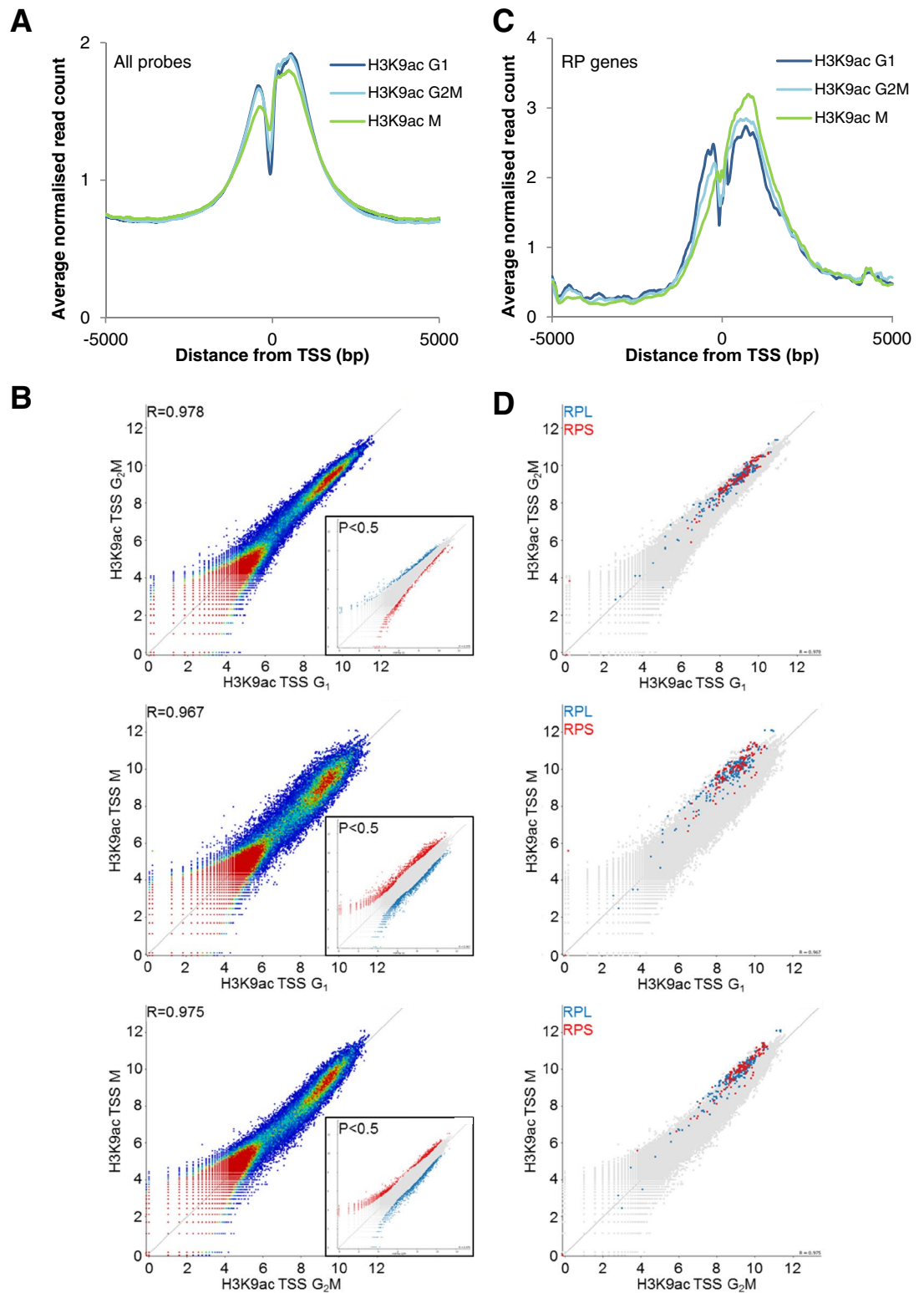


**Figure 7.** Transcription start sites of ribosomal protein genes are enriched in H3K9ac in mitosis in HeLa cells. (A) HeLa cells were sorted by centrifugal elutriation (G<sub>1</sub>, G<sub>2</sub>M) and mitotic shakeoff (M). Average distribution (average read count normalised to total read count) across a 10 kb window centred on all transcription start sites (TSS) is shown. (B) ChIP-seq signal at TSS (–500 bp to +750 bp) is compared between cell cycle phases. Significantly enriched TSS (P < 0.5) were identified by intensity difference as shown in the inset panels. (C) The average H3K9ac distribution across the TSS of ribosomal protein (RP) genes (large and small, excluding mitochondrial) is shown. (D) ChIP-seq signal at TSS of ribosomal protein genes is compared between cell cycle phases. RPL genes are shown in blue and RPS genes in red.

this gene family increased as cells progressed into G<sub>2</sub>, but levelled off towards the end of this phase, suggesting that the increase in activating modifications reflects on-going transcription. This conclusion is consistent with the finding that the increase in G<sub>2</sub>M of H3K9ac in the *gene body* is even more marked than the increase at TSS.

**A homeostatic mechanism conserves the genomic distribution of histone PTM.** Our results point to the existence of a homeostatic mechanism that serves to maintain levels of certain histone PTM at specific locations, through the cell cycle. This is a challenging proposition, not least because histone acetylation and methylation are both dynamic processes maintained by the balanced action of appropriately targeted modifying and de-modifying enzyme complexes<sup>1</sup>. Thus, the unchanging distribution and relative levels of H3K9ac, H3K4me3 and H3K27me3 through the cell cycle, requires an unchanging balance of specifically targeted enzyme activities. This may be achieved, at least in part, through the presence of domains recognizing specific PTMs (“reader” domains) in enzyme complexes responsible for placing that same PTM<sup>59</sup>. There are now many examples of this, along with an increasing awareness of the functional and structural consequences of complex interactions between different modifications, “crosstalk”<sup>1</sup>. Modifications that show very little cell-cycle-dependent change, such as H3K9ac, must be managed alongside those that change rapidly at specific cell cycle stages, such as H3S10ph in G<sub>2</sub><sup>24–26</sup>. These considerations make it unlikely that levels of modifications such as H3K9ac are conserved solely through adoption of a chromatin configuration that excludes the relevant enzymes. Nor can the maintenance of patterns of modification be attributed solely to on-going transcription, important though this may be in particular cases, such as mitotic genes expressed in G<sub>2</sub> (see above).

Previous data support the existence of an intrinsic cellular mechanism conserving levels of at least some histone modifications. Treatment of cultured cells with HDAC inhibitors (HDACi) such as sodium butyrate, causes little or no increase in histone acetylation across most genes tested, despite global histone hyperacetylation<sup>60,61</sup>. Further, within 60 min of exposure to HDACi, we noted decreased transcription of genes encoding essential components of all known HAT complexes, a change suggestive of a homeostatic process aimed at conserving levels of histone acetylation. The initially surprising inability of HDACi to induce hyperacetylation at most gene promoters is consistent with the limited transcriptional response to HDACi, and the fact that genes that do respond can be up- or down-regulated<sup>62–64</sup>. Such global controls would complement the more local mechanisms responsible for the self-perpetuation of histone modifications discussed earlier.

**Maintenance of cell-type-specific transcription patterns through mitosis.** It has been proposed that patterns of expression of at least some genes are conserved through mitosis by the retention of selected transcription factors at the promoter regions<sup>19,20,65,66</sup>. The hypothesis has been termed bookmarking, and recent work has shown that it can involve not only TFs, but enzymes such as the p300 complex<sup>67</sup> and poly [ADP-ribose] polymerase I<sup>68</sup>, nucleosomes<sup>69</sup> and histone PTM<sup>70</sup>, see<sup>71</sup> for a recent review. These findings are all compatible with the multiple levels of control that we now know to be involved in transcriptional regulation in eukaryotes.

Transcription of most genes is suppressed through mitosis<sup>72</sup> though there are interesting exceptions<sup>73,74</sup> and transcription of some genes restarts before cell division is complete<sup>75</sup>. There is a general reduction in histone acetylation as cells move into mitosis, driven largely by the actions of histone deacetylases<sup>76</sup>. Moreover, turnover of various histone acetates is diminished in metaphase HeLa cells, as measured by the minimal hyperacetylation induced by treatment with HDAC inhibitors<sup>77</sup>. Despite this overall change in turnover rate, we see very little change in the *relative* levels of modification of the regions studied here. A notable exception is provided by the ribosomal protein (RP) genes in HeLa cells, whose TSS show consistently high levels of H3K9ac in metaphase. It is unclear why these very highly expressed housekeeping genes<sup>78</sup> should respond differently to other genes or genomic domains, but it is significant that all the RP genes we have tested respond in the same way. The balanced expression of the 80 members of the RP gene family is essential for efficient ribosome biogenesis<sup>79</sup>. Thus, although the functional significance of the increased H3K9ac at RP gene promoters remains unknown, it is of interest that all members of the family tested showed the same characteristic marking through metaphase. It may be that, in HeLa cells, the demand for ribosomal proteins is such that transcription of RP genes, unusually, persists through mitosis, accounting for the relatively increased H3K9ac levels. Alternatively, the relatively high levels of H3K9ac may facilitate the rapid up-regulation of RP gene transcription as cell exit mitosis. These possibilities will be explored.

A model summarising our results so far is shown in Fig. 8. It shows how cell-type-specific patterns of histone PTM, specifically acetylation, persist through the cell cycle in the form of regions within the 5–1000 Kb range (here designated sub-bands) that show characteristically high or low levels of modification depending on the cell type. The model makes two additional proposals. First, that histone acetylation facilitates the assembly of similarly marked chromatin regions into sub-nuclear structures, (functional domains) configured so as to enhance or diminish transcription of the genes within them. And second, that persistence of regional histone acetylation through metaphase, albeit at a reduced level, guides the reassembly of cell-type-specific structures as cells exit mitosis. As noted earlier, there is a strong, causal relationship between levels of histone acetylation and the ability of chromatin to condense, by phase separation, into sub-structures visible at the light microscope level and able to influence transcription of incorporated genes<sup>14</sup>.

Consistent with possibilities outlined in Fig. 8, we find that histone modifications associated with TADs<sup>15,16</sup> show cell-specific differences and are highly conserved through the cell cycle including, in the case of H3K9ac and HeLa cells, passage through metaphase. This is significant in that TADs are undetectable by chromatin conformation capture in metaphase HeLa cells, but reappear a few hours into G<sub>1</sub><sup>18</sup>. Perhaps persistent patterns of H3K9ac and other histone PTM provide markers that allow the re-establishment of TADs after mitosis. A similar suggestion has been made very recently by Kang et al.<sup>75</sup> following a detailed study correlating the distribution

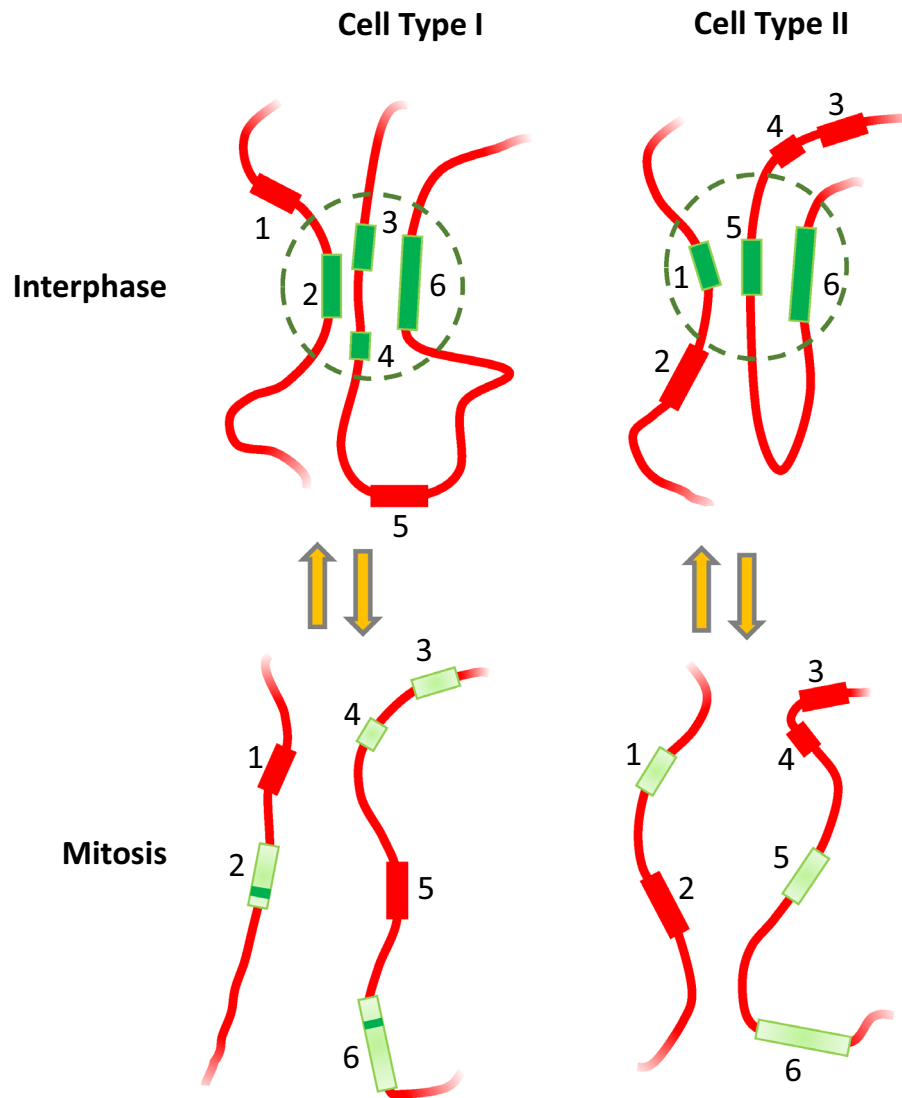


**Figure 8.** Cell-type-specific patterns of histone acetylation persist through the cell cycle and may guide the reformation of functional chromatin domains as cells leave mitosis. The coloured rectangles numbered 1–6 indicate chromosomal regions within the 5–1000 Kb size range that are marked by relatively high levels of histone acetylation (shown in green) in at least one of the two cell types studied (LCL and HeLa). Such regions are referred to in the text as sub-bands. Intervening chromatin showing a consistently low level of acetylation is shown in red, as are sub-bands that are weakly acetylated in one cell type or the other. Sub-bands 1–2 and 3–6 may be on the same or different chromosomes. In interphase, highly acetylated sub-bands can associate to form functional domains (dashed circles) that differ between cell types. Functional domains may be characterised by a particular level of transcriptional activity. At least some functional domains dissociate through mitosis, much as TADs are known to do. There is a global fall in histone acetylation as cells move through mitosis, but our results show that the highly acetylated sub-bands that characterize each cell type remain *relatively* highly acetylated in mitotic cells (shown in pale green). In addition, some genes (e.g. all Ribosomal Protein genes so far tested in HeLa cells) seem to escape global deacetylation, thus showing up as particularly highly acetylated in metaphase (marked as narrow transverse strips in sub-bands 2 and 6 in Cell Type I only). We suggest that the relatively high levels of histone acetylation, and perhaps other histone PTM, within particular sub-bands form part of a mechanism that guides the reformation of cell-type-specific transcriptional domains, and hence patterns of gene expression, as cells leave mitosis.

of H3K27ac, H3K4me1 and H3K4me3 through mitosis and the reappearance of TADs and cell-specific gene expression in G<sub>1</sub>.

It seems inevitable that multiple interacting mechanisms contribute to the maintenance of cell type specific patterns of gene expression through the cell cycle. The extraordinarily precise conservation through the cell

cycle of the genomic distribution of histone PTM, specifically H3K9ac, H3K4me3 and H3K27me3, indicates their close involvement in this process.

## Conclusions

Genome-wide analysis by ChIP-seq, shows histone modifications H3K4me3, H3K9ac and H3K27me3 to be relatively enriched over chromosomal domains of 10–50 Mb. These domains do not differ detectably between cell types, do not vary through the cell cycle and correspond to bands detectable by immunofluorescence microscopy of metaphase chromosome spreads. The relatively high levels of both activating and silencing histone PTM in these regions are likely to be by-products of their high gene density.

By ChIP-seq, these regions are made up of clearly defined sub-regions of 2–5 MB or less. These sub-regions differ between cell types but are invariant through the cell cycle.

Analysis of individual promoter regions confirmed a general lack of variation through the cell cycle within each cell type, the only exceptions being genes whose transcription was up-regulated in G<sub>2</sub> in order to generate proteins required for passage through mitosis.

Our results suggest that H3K4me3, H3K9ac and H3K27me3 are components of a homeostatic mechanism by which chromatin states responsible for cell-type-specific patterns of gene expression are set and maintained through the cell cycle.

## Methods

**Cell culture.** The AH-LCL lymphoblastoid cell line was established by Rowe et al.<sup>80</sup> and was cultured in RPMI 1640 medium, 10% foetal bovine serum, supplemented with L-glutamine (2 mM) and penicillin/streptomycin (all reagents from Life Technologies) at 37 °C, 5% CO<sub>2</sub>. HeLa cells were cultured in DMEM medium supplemented with 10% foetal bovine serum (Sigma), supplemented with L-glutamine (2 mM) and penicillin/streptomycin (Life Technologies). The human/mouse hybrid cell line GM11941, containing human chromosome 11 was purchased from the Coriell Institute and cultured in RPMI 1640 medium, 10% foetal bovine serum, supplemented with L-glutamine (2 mM) and penicillin/streptomycin. All cell lines were regularly tested for mycoplasma.

**Cell sorting methods.** *Flow cytometry.* 1 × 10<sup>8</sup> LCL yielded approximately 6 × 10<sup>6</sup> G<sub>2</sub>M cells from a 4-h sort. Cells were treated with 0.1 µg/ml colcemid for 4 h to enrich the mitotic fraction. Cells were then harvested by centrifugation and washed three times in PBS. Ice cold acetone was added dropwise to ~ 1 × 10<sup>7</sup> cells/ml on a very slow vortex before freezing to – 20 °C for at least 2 h. Cells were then centrifuged at 30×g for 10mins, 4 °C (MSE chillspin), acetone was carefully removed from the pellet and ice-cold PBS was added dropwise to ~ 1 × 10<sup>7</sup> cells/ml. The cells were centrifuged and resuspended in PBS at 2 × 10<sup>7</sup> cells/ml. Propidium iodide was added to a concentration of 10 µg/ml and incubated for 30 min at 4 °C. Cells were sorted into G<sub>1</sub> and G<sub>2</sub>M fraction based on Propidium iodide fluorescence using a MoFlo cell sorter (DakoCytomation).

*Centrifugal elutriation.* Centrifugal elutriation was carried out using a JE-5.0 elutriating centrifuge (Beckman Coulter) as described by Banfalvi<sup>81</sup>. 3 × 10<sup>8</sup> LCL were harvested by centrifugation and resuspended in 10 ml elutriation buffer (5 mM EDTA, 1% bovine serum albumin in 0.75 × PBS); HeLa cells were trypsinised, washed in culture medium and 3 × 10<sup>8</sup> cells resuspended in 10 ml of elutriation. A single cell suspension was achieved by passage through an 18G needle and cells were loaded into the elutriation chamber. For LCL, loading was at a flow rate of 11 ml/min and a rotor speed of 1800 rpm. For HeLa cells, the optimal G<sub>1</sub> fractions was achieved loading at 15 ml/min, 1800 rpm and the purest G<sub>2</sub>M fraction at 11 ml/min, 1300 rpm. Cell cycle fractions were eluted by gradually (1 ml/min/min) increasing the flow rate and collecting 200 ml fractions at ~ 3 ml/min increments. Eluted cells were centrifuged and acetone-fixed as above for ChIP-seq. A sample of each fraction was fixed in 70% ethanol and cell cycle stage determined by propidium iodide staining and flow cytometry.

*Mitotic shake-off.* HeLa cells were grown on 15 cm culture plates (Corning), ensuring they were in log phase and no more than 70% confluent at time of shake off. Plates were shaken on an orbital shaker at 200 rpm for 1 min. Medium containing shaken-off cells was collected and cells pelleted by centrifugation. The first shake-off was discarded as it contained any dead cells and debris. Several subsequent shake-offs were carried out for each set of culture plates at intervals of 1 h. Mitotic samples were collected for ChIP-seq or replated for synchronous progression into G<sub>1</sub>. After the desired culture time, replated cells were detached by trypsinisation and washed in growth medium followed by PBS. Cells pellets were frozen prior to extraction for western blotting. Cells were acetone-fixed as above for ChIP-seq. A sample of each fraction was fixed in 70% ethanol and cell cycle stage determined by propidium iodide staining and flow cytometry.

**Antibodies.** Rabbit polyclonal antisera to H3K9ac (R607) and H3K4me3 (R612) were raised in-house by immunisation with synthetic peptides conjugated to ovalbumin as previously described<sup>8</sup>. Antibody specificities was assayed by inhibition ELISA and checked by Western blotting. The antibody to H3K27me3 was from Millipore (07-449).

**Chromatin immunoprecipitation-sequencing.** Immunoprecipitation of native chromatin was performed based on the method described previously<sup>82</sup>, with modifications but using acetone-fixed cells as described above. Acetone fixation permeabilises cell and nuclear membranes, removing the need to isolate nuclei prior to micrococcal nuclease digestion. Instead, acetone-fixed cells were washed twice in cold PBS and resuspended

in digestion buffer (0.32 M sucrose, 50 mM Tris/HCl (pH7.4), 4 mM MgCl<sub>2</sub>, 1 mM CaCl<sub>2</sub>, 5 mM Na Butyrate, 0.1 mM PMSF) at  $8 \times 10^7$  cells/ml (G<sub>1</sub>) or  $4 \times 10^7$  cells/ml (G<sub>2</sub>M). Micrococcal nuclease was added to 25units/ml and chromatin digested at 37 °C for 5 min. The reaction was stopped by the addition of EDTA to 5 mM. Chromatin was pre-cleared by incubation with protein A sepharose beads and incubated overnight with antibodies to H3K9ac, H3K4me3 and H3K27me3. Antibody-bound material was isolated on Protein A-Sepharose beads (Invitrogen, UK) and DNA from antibody-bound and input chromatin was purified by PCR purification kit (Qiagen). Sequencing libraries were prepared from 100 ng DNA per sample using the NEBNext Library preparation kit for Illumina (NEB). Samples were barcoded using the system described by Bronner et al.<sup>83</sup>. Fragments were amplified with 12–18 cycles using adaptor specific primers (Illumina); fragments ranging between 300 and 500 bp in size were gel-purified before cluster generation and sequencing. Sequencing was carried out at the Babraham Institute, Cambridge on an Illumina Genome Analyzer GAIIX using Cluster Generation v4 chemistries and Sequencing by Synthesis Kit v4. Data collection was performed using Sequencing Control Software v2.6. Real-time Analysis (RTA) 1.5–1.8 were used for base calling. ChIP-seq data was analysed using SeqMonk (Babraham Institute, <http://www.bioinformatics.babraham.ac.uk/projects/seqmonk/>). Input samples were checked for uniform coverage and ChIP samples normalised for read count to the largest data store.

**Immunofluorescence.** Metaphase chromosome spreads were prepared and immunostained as previously described<sup>32</sup>. Briefly, cells were treated for two hours with colcemid at 0.1 µg/ml. Cells were washed twice with cold PBS and swollen in 75 mM KCl at  $2 \times 10^5$  cells/ml at room temperature for 10 min. 200 µl aliquots of the swollen cell suspension were spun onto glass slides at 1800 rpm for 10 min in a Shandon Cytospin 4. Slides were immersed for 10 min. at room temperature in KCM buffer (120 mM KCl, 20 mM NaCl, 10 mM Tris/HCl pH 8.0, 0.5 mM EDTA, 0.1% Triton X-100). Immunolabelling was carried out for 1 h at 4 °C with antisera diluted 200–400 fold in KCM supplemented with 1–1.5% BSA. The secondary antibody was FITC-conjugated goat anti-rabbit immunoglobulin (Sigma F1262) diluted 150-fold in KCM, 1% BSA. Slides were washed twice in KCM (5 min. at room temperature), fixed in 4% v/v formaldehyde (10 min. at room temperature), rinsed in deionised water and mounted in Vector Shield (Vector lab) supplemented with DAPI (Sigma) at 2 µg/ml. Slides were visualized on a Zeiss Axioplan 2 epifluorescence microscope.

**RT-PCR.** RNA was extracted from elutriated LCL fractions using the RNeasy mini kit (Qiagen), including on column DNase I digestion, and converted to cDNA using Tetro cDNA synthesis kit (Bioline) according to the manufacturer's instructions. Realtime RT-PCR was carried out on an Applied Biosystems 7900HT using SensiMix SYBR green master mix (Bioline). 300 nM each primer were added to 10 µl reactions in 384-well plates. Primers were designed to amplify unspliced pre-mRNA. Primer sequences are given in Supplementary Table S3. Experiments were carried out in triplicate and 3 technical replicates were set up for each qPCR reaction. Statistical significance was determined by T-Test relative to the F125 fraction.

**Gene expression microarray.** LCL cells were harvested by centrifugation. HeLa cells were shaken off in mitosis as above, replated and grown for a further 4 h (mid G<sub>1</sub>) before harvesting by trypsinisation. RNA was extracted and purified using the RNeasy kit with DNase digestion (Qiagen) according to the manufacturer's instructions. Double stranded cDNA was synthesised using the cDNA Synthesis System (Roche-Nimblegen), including RNase I and Proteinase K treatment followed by DNA clean up using the PCR purification kit (Qiagen). Samples were labelled with cy3 using a One-Colour Labeling Kit (Roche-Nimblegen), mixed with alignment oligos and sample tracking control oligos (Nimblegen Hybridisation and Sample Tracking Control Kits) and hybridised to a 12 × 135 k HD2 expression array (Roche Nimblegen, containing 3 probes per sequence for 44,049 human sequences) and scanned on a Nimblegen MS200 Microarray scanner. Data were extracted using DEVA (Roche Nimblegen) and normalised by robust multichip average in R<sup>84</sup>. Ontology analysis was carried out using DAVID<sup>85</sup>.

### Data availability

Expression microarray data and ChIP-sequencing datasets are available at GEO, accession numbers GSE163546, GSE165237 and GSE24459.

Received: 2 November 2020; Accepted: 18 January 2021

Published online: 04 February 2021

### References

- Bannister, A. J. & Kouzarides, T. Regulation of chromatin by histone modifications. *Cell Res.* **21**, 381–395 (2011).
- Dunham, I. *et al.* An integrated encyclopedia of DNA elements in the human genome. *Nature* **489**, 57–74 (2012).
- Heintzman, N. D. *et al.* Distinct and predictive chromatin signatures of transcriptional promoters and enhancers in the human genome. *Nat. Genet.* **39**(3), 311–318 (2007).
- Pauler, F. M. *et al.* H3K27me3 forms BLOCs over silent genes and intergenic regions and specifies a histone banding pattern on a mouse autosomal chromosome. *Genome Res.* **19**, 221–233 (2009).
- Ringrose, L. Polycomb comes of age: genome-wide profiling of target sites. *Curr. Opin. Cell Biol.* **1**, 290–297 (2007).
- Mir, M., Bickmore, W., Furlong, E. E. M. & Narlikar, G. Chromatin topology, condensates and gene regulation: Shifting paradigms or just a phase? *Development* **1**, 146 (2019).
- Strom, A. R. *et al.* Phase separation drives heterochromatin domain formation. *Nature* **547**, 241–245 (2017).
- Larson, A. G. *et al.* Liquid droplet formation by HP1a suggests a role for phase separation in heterochromatin. *Nature* **547**, 236–240 (2017).
- Tatavosian, R. *et al.* Nuclear condensates of the Polycomb protein chromobox 2 (CBX2) assemble through phase separation. *J Biol Chem.* **294**, 1451–1463 (2019).

10. Plys, A. J. *et al.* Phase separation of polycomb-repressive complex 1 is governed by a charged disordered region of CBX2. *Genes Dev.* **33**, 799–813 (2019).
11. Sabari, B. R. *et al.* Coactivator condensation at super-enhancers links phase separation and gene control. *Science* **361**, 3958 (2018).
12. Cho, W. K. *et al.* Mediator and RNA polymerase II clusters associate in transcription-dependent condensates. *Science* **361**, 412–415 (2018).
13. Lu, H. *et al.* Phase-separation mechanism for C-terminal hyperphosphorylation of RNA polymerase. *Science* **II**(1), 1–20 (2018).
14. Gibson, B. A. *et al.* Organization of chromatin by intrinsic and regulated phase separation. *Cell* **179**, 470–484 (2019).
15. Dixon, J. R. *et al.* Topological domains in mammalian genomes identified by analysis of chromatin interactions. *Nature* **485**, 376–380 (2012).
16. Rao, S. S. P. *et al.* A 3D map of the human genome at kilobase resolution reveals principles of chromatin looping. *Cell* **159**, 1665–1680 (2014).
17. Chen, Y., Wang, Y., Xuan, Z., Chen, M. & Zhang, M. Q. De novo deciphering three-dimensional chromatin interaction and topological domains by wavelet transformation of epigenetic profiles. *Nucleic Acids Res.* **44**, 10 (2016).
18. Naumova, N. *et al.* Organization of the mitotic chromosome. *Science* **342**, 948–953 (2013).
19. Martínez-Balbás, M. A., Dey, A., Rabindran, S. K., Ozato, K. & Wu, C. Displacement of sequence-specific transcription factors from mitotic chromatin. *Cell* **83**, 29–38 (1995).
20. Kadauke, S. & Blobel, G. A. *Mitotic Bookmarking by Transcription Factors* (Springer, New York, 2013).
21. Ginno, P. A., Burger, L., Seebacher, J., Iesmantavicius, V. & Schübeler, D. Cell cycle-resolved chromatin proteomics reveals the extent of mitotic preservation of the genomic regulatory landscape. *Nat. Commun.* **9**, 10 (2018).
22. Reverón-Gómez, N. *et al.* Accurate recycling of parental histones reproduces the histone modification landscape during DNA replication. *Mol. Cell.* **72**(239–249), e5 (2018).
23. Alabert, C. *et al.* Two distinct modes for propagation of histone PTMs across the cell cycle. *Genes Dev.* **29**, 585–590 (2015).
24. Wei, Y., Yu, L., Bowen, J., Gorovsky, M. A. & David, A. C. Phosphorylation of histone H3 is required for proper chromosome condensation and segregation. *Cell* **97**, 99–109 (1999).
25. Wei, Y., Mizzen, C. A., Cook, R. G., Gorovsky, M. A. & Allis, C. D. Phosphorylation of histone H3 at serine 10 is correlated with chromosome condensation during mitosis and meiosis in *Tetrahymena*. *Proc. Natl. Acad. Sci. USA.* **95**, 7480–7484 (1998).
26. Sauvé, D. M., Anderson, H. J., Ray, J. M., James, W. M. & Roberge, M. Phosphorylation-induced rearrangement of the histone H3 NH2-terminal domain during mitotic chromosome condensation. *J. Cell. Biol.* **145**, 225–235 (1999).
27. Goto, H. *et al.* Identification of a novel phosphorylation site on histone H3 coupled with mitotic chromosome condensation. *J. Biol. Chem.* **274**, 25543–25549 (1999).
28. Polioudaki, H. *et al.* Mitotic phosphorylation of histone H3 at threonine 3. *FEBS Lett.* **560**, 39–44 (2004).
29. Fischle, W., Wang, Y. & Allis, C. D. Binary switches and modification cassettes in histone biology and beyond. *Nature* **425**, 475–479 (2003).
30. Jeppesen, P., Mitchell, A., Turner, B. & Perry, P. Antibodies to defined histone epitopes reveal variations in chromatin conformation and underacetylation of centric heterochromatin in human metaphase chromosomes. *Chromosoma* **101**, 322–332 (1992).
31. Cimini, D., Mattiuzzo, M., Torosantucci, L. & Degrossi, F. Histone hyperacetylation in mitosis prevents sister chromatid separation and produces chromosome segregation defects. *Mol. Biol. Cell.* **14**, 3821–3833 (2003).
32. Terrenoire, E. *et al.* Immunostaining of modified histones defines high-level features of the human metaphase epigenome. *Genome Biol.* **11**, R110 (2010).
33. Pope, B. D., Hiratani, I. & Gilbert, D. M. Domain-wide regulation of DNA replication timing during mammalian development. *Chromosom. Res.* **1**, 127–136 (2010).
34. Bickmore, W. A. Patterns in the genome. *Heredity* **123**, 50–57 (2019).
35. Terrenoire, E., Halsall, J. A. & Turner, B. M. Immunolabelling of human metaphase chromosomes reveals the same banded distribution of histone H3 isoforms methylated at lysine 4 in primary lymphocytes and cultured cell lines. *BMC Genet.* **16**, 1–10 (2015).
36. Ernst, J. *et al.* Mapping and analysis of chromatin state dynamics in nine human cell types. *Nature* **473**, 43–49 (2011).
37. Bernstein, B. E. *et al.* A bivalent chromatin structure marks key developmental genes in embryonic stem cells. *Cell* **125**, 315–326 (2006).
38. Pan, G. *et al.* Whole-genome analysis of histone H3 lysine 4 and lysine 27 methylation in human embryonic stem cells. *Cell Stem Cell* **1**, 299–312 (2007).
39. Zhao, X. D. *et al.* Whole-genome mapping of histone H3 Lys4 and 27 trimethylations reveals distinct genomic compartments in human embryonic stem cells. *Cell Stem Cell* **1**, 286–298 (2007).
40. Grandy, R. A. *et al.* Genome-wide studies reveal that H3K4me3 modification in bivalent genes is dynamically regulated during the pluripotent cell cycle and stabilized upon differentiation. *Mol. Cell Biol.* **36**, 615–627 (2016).
41. Thiecke, M. J. *et al.* Cohesin-dependent and -independent mechanisms mediate chromosomal contacts between promoters and enhancers. *Cell Rep.* **32**, 1–10 (2020).
42. Wutz, G. *et al.* Topologically associating domains and chromatin loops depend on cohesin and are regulated by CTCF, WAPL, and PDS5 proteins. *EMBO J.* **36**, 3573–3599 (2017).
43. The ENCODE Project Consortium. The ENCODE (encyclopedia of DNA elements) project. *Science* **306**, 636–640 (2004).
44. Yuan, G. C. *et al.* Molecular biology: Genome-scale identification of nucleosome positions in *S. cerevisiae*. *Science* **309**, 626–630 (2005).
45. Schmucker, S. & Sumara, I. Molecular dynamics of PLK1 during mitosis. *Mol. Cell. Oncol.* **1**, e954507 (2014).
46. Cheutin, T. & Cavalli, G. Progressive polycomb assembly on H3K27me3 compartments generates Polycomb bodies with developmentally regulated motion. *PLoS Genet.* **8**, 1–10 (2012).
47. Rowley, M. J. *et al.* Evolutionarily conserved principles predict 3D Chromatin organization. *Mol. Cell.* **67**, 837–852 (2017).
48. Chen, Y. *et al.* Mapping 3D genome organization relative to nuclear compartments using TSA-Seq as a cytological ruler. *J. Cell Biol.* **217**, 4025–4048 (2018).
49. Bickmore, W. A. & Van Steensel, B. Genome architecture: Domain organization of interphase chromosomes. *Cell* **1**, 1270–1284 (2013).
50. Banani, S. F., Lee, H. O., Hyman, A. A. & Rosen, M. K. Biomolecular condensates: Organizers of cellular biochemistry. *Nat. Rev. Mol. Cell Biol.* **18**, 285–298 (2017).
51. Erdel, F. & Greene, E. C. Generalized nucleation and looping model for epigenetic memory of Histone modifications. *Proc. Natl. Acad. Sci. USA.* **113**, E4180–E4189 (2016).
52. McSwiggen, D. T. *et al.* Evidence for DNA-mediated nuclear compartmentalization distinct from phase separation. *Elife.* **8**, 1–5 (2019).
53. Erdel, F. & Rippe, K. Formation of chromatin subcompartments by phase separation. *Biophys. J.* **1**, 2262–2270 (2018).
54. Jabbari, K., Chakraborty, M. & Wiehe, T. DNA sequence-dependent chromatin architecture and nuclear hubs formation. *Sci. Rep.* **9**, 1–11 (2019).
55. Sina, A. A. I. *et al.* Epigenetically reprogrammed methylation landscape drives the DNA self-assembly and serves as a universal cancer biomarker. *Nat. Commun.* **9**, 1–13 (2018).
56. Bickmore, W. & Pombo, A. Editorial overview: Genome architecture and expression. *Curr. Opin. Genet. Dev.* **1**, iii–iv (2019).

57. Hansen, A. S., Cattoglio, C., Darzacq, X. & Tjian, R. Recent evidence that TADs and chromatin loops are dynamic structures. *Nucleus* **1**, 20–32 (2018).
58. Gibcus, J. H. *et al.* A pathway for mitotic chromosome formation. *Science* **359**, 1–10 (2018).
59. Turner, B. M. Cellular memory and the histone code. *Cell* **1**, 285–291 (2002).
60. Halsall, J., Gupta, V., O'Neill, L. P., Turner, B. M. & Nightingale, K. P. Genes are often sheltered from the global histone hyperacetylation induced by HDAC inhibitors. *PLoS ONE* **7**, e33453 (2012).
61. Halsall, J. A., Turan, N., Wiersma, M. & Turner, B. M. Cells adapt to the epigenomic disruption caused by histone deacetylase inhibitors through a coordinated, chromatin-mediated transcriptional response. *Epigenet. Chrom.* **8**, 29 (2015).
62. Peart, M. J. *et al.* Identification and functional significance of genes regulated by structurally different histone deacetylase inhibitors. *Proc. Natl. Acad. Sci. USA* **102**, 3697–3702 (2005).
63. Van Lint, C., Emiliani, S. & Verdin, E. The expression of a small fraction of cellular genes is changed in response to histone hyperacetylation. *Gene Exp.* **5**, 245–253 (1996).
64. Rada-Iglesias, A. *et al.* Butyrate mediates decrease of histone acetylation centered on transcription start sites and down-regulation of associated genes. *Genome Res.* **17**, 708–719 (2007).
65. Michelotti, E. F., Sanford, S. & Levons, D. Marking of active genes on mitotic chromosomes. *Nature* **388**, 895–899 (1997).
66. John, S. & Workman, J. L. Bookmarking genes for activation in condensed mitotic chromosomes. *BioEssays* **20**, 275–279 (1998).
67. Wong, M. M. *et al.* Promoter-bound p300 complexes facilitate post-mitotic transmission of transcriptional memory. *PLoS ONE* **9**, e99989 (2014).
68. Lodhi, N., Kossenkov, A. V. & Tulin, A. V. Bookmarking promoters in mitotic chromatin: Poly(ADP-ribose)polymerase-1 as an epigenetic mark. *Nucleic Acids Res.* **42**, 7028–7038 (2014).
69. Kelly, T. K. *et al.* H2AZ maintenance during mitosis reveals nucleosome shifting on mitotically silenced genes. *Mol. Cell.* **39**, 901–911 (2010).
70. Liu, Y. *et al.* Widespread mitotic bookmarking by histone marks and transcription factors in pluripotent. *Stem Cells* **1**, 1–10 (2017).
71. Zaidi, S. K. *et al.* Mitotic gene bookmarking: An epigenetic program to maintain normal and cancer phenotypes. *Mol. Cancer Res.* **1**, 1617–1624 (2018).
72. Parsons, G. G. & Spencer, C. A. Mitotic repression of RNA polymerase II transcription is accompanied by release of transcription elongation complexes. *Mol. Cell. Biol.* **17**, 5791–5802 (1997).
73. Palozola, K. C. *et al.* Mitotic transcription and waves of gene reactivation during mitotic exit. *Science* **358**, 119–122 (2017).
74. Zaret, K. S. Genome reactivation after the silence in mitosis: Recapitulating mechanisms of development?. *Dev. Cell.* **29**, 132–144 (2014).
75. Kang, H. *et al.* Dynamic regulation of histone modifications and long-range chromosomal interactions during postmitotic transcriptional reactivation. *Genes Dev.* **34**, 1–18 (2020).
76. Attieh, Y. *et al.* Low frequency of H33 mutations and upregulated DAXX expression in MDS. *Blood* **121**, 4009–5011 (2013).
77. Patzlaff, J. S., Terrenoire, E., Turner, B. M., Earnshaw, W. C. & Paulson, J. R. Acetylation of core histones in response to HDAC inhibitors is diminished in mitotic HeLa cells. *Exp. Cell. Res.* **316**, 2123–2135 (2010).
78. Bohnsack, K. E. & Bohnsack, M. T. Uncovering the assembly pathway of human ribosomes and its emerging links to disease. *EMBO J.* **38**, 1–10 (2019).
79. Gupta, V. & Warner, J. R. Ribosome-omics of the human ribosome. *RNA* **20**, 1004–1013 (2014).
80. Rowe, M. *et al.* Epstein-Barr virus (EBV)-associated lymphoproliferative disease in the SCID mouse model: Implications for the pathogenesis of EBV-positive lymphomas in man. *J. Exp. Med.* **173**, 147–158 (1991).
81. Banfalvi, G. Cell cycle synchronization of animal cells and nuclei by centrifugal elutriation. *Nat. Protoc.* **3**, 663–673 (2008).
82. O'Neill, L. P. & Turner, B. M. Immunoprecipitation of native chromatin: NChIP. *Methods* **31**, 76–82 (2003).
83. Bronner, I. F., Quail, M. A., Turner, D. J. & Swerdlow, H. Improved protocols for Illumina sequencing. *Curr. Protoc. Hum. Genet.* **80**, 1–10 (2014).
84. Saeed, A. I. *et al.* TM4: A free, open-source system for microarray data management and analysis. *Biotechniques* **34**, 374–378 (2003).
85. Huang, D. W., Sherman, B. T. & Lempicki, R. A. Systematic and integrative analysis of large gene lists using DAVID bioinformatics resources. *Nat. Protoc.* **4**, 44–57 (2009).

## Acknowledgements

We are grateful to Rebecca Sie for technical support. We thank Amanda Fisher for encouraging us to try the centrifugal elutriation approach and Roger Grand for unearthing a suitable rotor.

## Author contributions

J.A.H. designed and carried out experiments, analysed the data and wrote the manuscript, S.A. analysed the data, F.K. analysed the data, C.E.R. carried out experiments, G.F. carried out sequencing, W.R. advised on study design and supported sequencing, B.M.T. conceived the study, designed experiments, analysed the data and wrote the manuscript.

## Funding

This work was supported in its early stages by Grants from Cancer Research UK (C1015/A13794).

## Competing interests

The authors declare no competing interests.

## Additional information

**Supplementary Information** The online version contains supplementary material available at <https://doi.org/10.1038/s41598-021-82539-z>.

**Correspondence** and requests for materials should be addressed to J.A.H. or B.M.T.

**Reprints and permissions information** is available at [www.nature.com/reprints](http://www.nature.com/reprints).

**Publisher's note** Springer Nature remains neutral with regard to jurisdictional claims in published maps and institutional affiliations.



**Open Access** This article is licensed under a Creative Commons Attribution 4.0 International License, which permits use, sharing, adaptation, distribution and reproduction in any medium or format, as long as you give appropriate credit to the original author(s) and the source, provide a link to the Creative Commons licence, and indicate if changes were made. The images or other third party material in this article are included in the article's Creative Commons licence, unless indicated otherwise in a credit line to the material. If material is not included in the article's Creative Commons licence and your intended use is not permitted by statutory regulation or exceeds the permitted use, you will need to obtain permission directly from the copyright holder. To view a copy of this licence, visit <http://creativecommons.org/licenses/by/4.0/>.

© The Author(s) 2021